Received: 15 January 2021 | Revised: 8 March 2021 | Accepted: 6 April 2021

DOI: 10.1049/rsn2.12093

IET Radar, Sonar & Navigation

The Institution of Engineering and Technology WILEY

ORIGINAL RESEARCH PAPER

# Eavesdropping like a bat: Towards fusing active and passive sonar for a case study in simultaneous localization and mapping

**Masoud Jahromi Shirazi**[1] | **Nicole Abaid**[2]

[1]Engineering Mechanics Program, Virginia Tech, Blacksburg, Virginia, USA

[2]Department of Mathematics, Virginia Tech, Blacksburg, Virginia, USA

**Correspondence**

Nicole Abaid, 460 McBryde Hall, Virginia Tech, 225 Stanger Street, Blacksburg, VA 24061-1026, USA. Email: nabaid@vt.edu

**Funding information**

National Science Foundation; United States, Grant/Award Number: 1751498; Unassigned

**Abstract**

Among so-called active sensors that use self-generated signals, sonar sensors are more challenging to implement than lidar and radar due in part to their limited angular field of sensing. A common solution to this challenge is scanning sensors that sweep an angular range with successive measurements. However, scanning sensors are particularly problematic for sonar because of the relatively slow sound speed and the inertia of the sonar head. Studies of bat behaviour suggest that bats may eavesdrop on their conspecifics during group flight. In other words, they fuse information gathered by their own active sonar with information they receive by passively listening to peers. Because bats are extremely skilled in using sonar, this behaviour inspired an investigation into whether fusing active and passive sonar can be a solution to the challenges of implementing sonar sensors. A model of fused sensing is defined, and a numerical simulation is used to answer this question on the test bed problem of simultaneous localization and mapping (SLAM). The simulation results show that when the angular range of active sonar and associated noise is relatively small, the robot's performance in solving SLAM is improved.

## 1 | INTRODUCTION

Sensors are integral components of any automated system responsible for providing information about the environment. Sensors can generally be categorized in two groups, *passive* and *active*. Passive sensors passively detect the signals generated by a source in the environment. A camera used for object detection is an example of a passive sensor because it detects the light beams generated by a source and reflected by the environment. In contrast, active sensors actively spend energy to generate a signal within the environment and use the returning reflections for perception [1]. Sonar, lidar, and radar are common examples of active sensors. Active sensors have an advantage over passive sensors in that they can operate in environments not rich with the type of energy the sensor's receiver can detect. As an example, using a camera flash to capture images when the environment is dark changes the camera into an active sensor. In addition, active sensors may provide more information about the environment due to time difference between sending the signal and receiving the reflection, known as *time of flight*, that is not available to passive sensors. However, active sensors require an energy source to generate signals to impose restrictions, especially on operating time. In multiagent applications, active sensors are prone to *signal jamming*, which refers to the confusion of the sensor in distinguishing the reflection of its own signal from that of its peers. This problem can be resolved by implementing a *matched filter* to filter out signals that do not match the signature of the sensor's own emitter by maximizing the signal-to-noise ratio [2].

In mobile robot applications, sonar is considered a particularly challenging sensor compared with lidar and radar. Sonar sensors, or so-called ultrasonic range finders, have slower data-acquisition rates than lidar due to the difference in the speeds of sound and light. Therefore, when the robot has high velocity, a sonar sensor will not be in the same nominal position at the transmitting and receiving times [3]. This can be modified if necessary by the approaches developed in bistatic sonar [4]. Moreover, in comparison with lidar, sonar has a wide beam width that makes it a less accurate ray-trace sensor with less angular resolution [5], particularly in air. In addition, because sound has a fairly long wavelength compared with the roughness of most surfaces (between 7 and 17 mm for a sound wave with a frequency between 20 and 50 kHz), the sound

usually reflects specularly in practical applications. Therefore, when the sound wave is not perpendicular to the surface, most of its energy specularly reflects away from the sensor or gets bounced back to the sensor from another object, leading to missed or incorrect range detection [3, 5–9]. For example, a plane is only visible if the angle between the sonar axis and the normal vector to the plane is less than the opening angle of the main lobe of the beam [10]. One proposed solution to these missed reflections is to use a sonar ring to make a grid of sonar sensors to cover the entire body of the robot [11]. However, the collected data can be dramatically affected by vehicle orientation [3].

A major challenge of sonar sensors is their directionality, that is, the sensor is only able to view what is in front of it (assuming that objects avoid specular reflection and yet can generate perceptible echoes). Although this may not be an important restriction in some applications such as obstacle avoidance, it can become critical in other tasks such as mapping or object classification [10]. One solution to this challenge is again the use of a sonar ring that emits sound waves in all directions. However, acoustic interference between neighbouring transducers can impose challenges and limit measurement sampling frequency, which may preclude online applications [11, 12]. Another solution is to use scanning sonar [3, 13], in which a single sensor takes multiple measurements from different vantage points. Having a wide beam width makes it hard to find the direction of an echo's return, as it is usually assumed that the return is coming from the central axis of the sonar. In addition to this limitation, scanning sonar suffers from a slow update rate, and therefore, the results are distorted by vehicle motion [3]. For example, it takes at least 6 s for Tritech MiniKing imaging sonar to complete a scan because of its mechanical limits, and this time can increase dramatically depending on the range setting; at a 50 m range setting, a complete scan takes about 15 s [14]. Despite these challenges, sonar sensors are popular in mobile robot applications because of their low cost [15]. Sonar sensors are mostly used in underwater applications because sound can travel farther underwater than radio waves and light [16]. These benefits of sonar make a strong case for its implementation in engineering applications.

Despite the challenging physics behind acoustics and sonar, some animals such as bats and dolphins successfully use sonar sensing in nature [17, 18]. Bat sonar involves only a transmitter, the larynx, and two ears as receivers, which is qualitatively simpler than the sonar rings and scanners mentioned above. Despite the simple structure their sonar, however, bats are able to implement it in a very sophisticated way. They can balance sensor range, opening angle, and spatial resolution using techniques such as modulating sound frequency [19], temporal shape of the sound wave signal [20], or sound direction [21]. To create and analyze acoustic signals, they may also actively move their nose leaves and pinnae, which has inspired engineers to build biomimetic emitters and receivers [22–24]. With multiple receivers, it is possible to localize a sound source based on the time difference of arrival of the sound to different receivers, as shown in the literature [25–27]. In robotics applications, this idea has been implemented using two receivers, which is referred to as *binaural sound source localization* [28], which can provide both range and bearing measurements. Motivated by bat sensing, several research groups have developed sonar sensors based on this idea [29–31].

Studies on bat group behaviour show other fascinating abilities of these animals that only manifest in group interactions. For example, it has been observed with a pair of flying bats that occasionally one stops making sounds, presumably to avoid signal jamming [32]. How can a bat navigate and avoid obstacles without using its sonar? Another study indicates that bats intentionally jam a peer's signal to compete for food [33]. Based on these studies, it seems that bats not only use their sonar actively but also passively obtain information by *eavesdropping* on their peers' calls. In other words, bats fuse the information they obtain through active and passive sonar to enhance their perception of the environment. This is not common in sonar sensing in autonomous vehicle applications, which raises the research question of whether this type of information fusion can be beneficial in that context. In particular, can this type of eavesdropping behaviour be a solution to the limitations of sonar directionality by covering the *blind spot* of an active sensor with information from passive sonar? This may lead to the elimination of the slow update rate inherent in scanning sonar or sonar rings.

To investigate the possible benefits of fusing active and passive sonar, we investigate the canonical robotics problem of landmark-based simultaneous localization and mapping (SLAM) using an extended Kalman filter (EKF) [34]. In this problem, a robot explores an unknown environment to build a map by finding the location of landmarks in the environment and simultaneously localizing itself within this map. The EKF, while widely used, is known to be a suboptimal algorithm. Researchers have investigated fusing information through different sensors or implementing different estimation algorithms to improve its performance [35, 36]. Inspired by eavesdropping in bats, we aim to investigate the effect of fusing the information of passive sonar with active sonar. Such information fusion is particularly interesting because it does not require the use of additional hardware. To this end, we use a Monte Carlo numerical simulation and evaluate the performance of the algorithm within a range of parameters and under three different scenarios: (1) a robot using only active sonar with range and bearing measurements, (2) a robot using only passive sonar with bearing measurements, and (3) a robot fusing active and passive sonar.

The rest of the paper is organized as follows. In Section 2, we formally define the problem, provide simplifying assumptions, and describe the simulation scenarios. In Section 3, we introduce the dynamic model of the robot. Section 4 describes the measurement models and the SLAM algorithm used in each sensing strategy. The simulation results are presented in Section 5, and Section 6 is devoted to concluding remarks and future work.

## 2 | PROBLEM STATEMENT

In this section, we explain the simulation scenario and the simplifying assumptions made. We should emphasize here that some of these simplifying assumptions are challenges that need to be addressed before solving SLAM in practice and are open-ended problems. However, to be able to study the effectiveness of fusing active and passive sonar in improving a robot's performance at this stage, we must make these simplifying assumptions. Once an improvement in a robot's performance is verified by this study, it justifies expending the research effort to solve these challenges.

The problem of SLAM is a well-studied problem in robotics. A ground robot is located in an unknown environment that has an unknown number of fixed-point landmarks at unknown locations. The objective of the robot is to build a map of landmark locations and localize itself within the map. A beacon emits sound waves in the environment at a known fixed frequency that will be reflected by the landmarks. We assume that the robot can receive the echoes of the beacon's sound reflected from the landmarks. This assumption is idealized in general because in real scenarios, the landmark may specularly reflect the sound, and the echo may not be received from some directions, or the robot may be located in the acoustic shadow of the landmark and not receive any signal. However, in a convex environment such as indoor applications with round landmarks or landmarks with rough surfaces that defuse the incident sound from the beacon, this assumption may be valid.

The ground robot is assumed to be equipped with a sonar emitter that can emit a sound at a different frequency than that of the beacon. Therefore, at the receiver, the robot can distinguish whether the received signal is a reflection of the beacon or its own emitter. The robot is able to measure the range to the landmark located within the region defined by its sensor opening, which is the angular range of the robot's receiver. Again, we assume that specular reflection does not prevent the sensor from missing the echo. In addition, it is assumed that the robot uses more than one receiver and is thus able to measure the bearing angle of the incident sound in a single measurement. With two receivers, it is possible to localize the bearing angle to the sound source by calculating the time difference of arrival of the incident sound to the receivers up to a cone—known as the cone of confusion—whose axis passes through both receivers. In two dimensions, the cone of confusion reduces to ambiguity between two points, one in the front and the other in the back of the receivers, which is referred to as front–back confusion [37]. There are several ways to resolve this confusion such as using consecutive measurements and performing probabilistic hypothesis testing [38, 39], implementing a head motion between two consecutive measurements to break symmetry [40], or exploiting the difference in frequency response of the receiver at different directions, usually referred to as the *head-related transfer function* in the acoustic and biology community studying humans and animals in the context of binaural sound localization [41, 42]. If the robot uses an array of at least three receivers, it can calculate the direction of the incident sound without any confusion [43], which is what we assume for this work.

Finally, the robot is assumed to be able to detect the echo of the beacon's sound reflected from nearby landmarks. This is the situation in our inspiring system of eavesdropping bats where two bats are flying close to each other and one acts as a beacon for the other. Therefore, one way to create such a situation is to make the beacon follow the robot. We can also assume that the environment is uniformly sonified by several beacons. This assumption is analogous to uniform lighting of the environment for the use of a camera.

The robot can operate in three different modes to solve the SLAM problem. In the first mode, the robot only detects the echo of its own emitted signals reflected from the environment and filters everything else, including the echoes generated by the beacon. We refer to this mode as *active SLAM*, which is the way current sonar sensors are implemented [3]. In this mode, the robot will have access to range and bearing measurements of all the landmarks located in the range of the emitter within its main lobe. In the second mode, the robot does not emit any signal and only uses the echoes of the beacon's sound. We call this mode *passive SLAM*. Because the robot lacks range information, it can only measure the bearing angle of the incident sound by comparing time differences in arrival between its receivers. In this way, it is similar to the bearing-only SLAM problem studied in the literature, for example, [44]. Finally, in the third mode, the robot uses its emitter and detects its echoes from landmarks as well as the echoes of the beacon's sound. In this case, the robot will have access to the range and bearing information of the actively located landmarks within the main lobe of the robot's emitter. For other landmarks detected passively through the beacon's echo, the robot will have access to bearing angle information only. This mode, which is a combination of active and passive sensing, resembles the eavesdropping behaviour observed in bats. We refer to this mode as *fused SLAM*.

In light of bat eavesdropping, the main research question of this work is whether combining active and passive sonar can be beneficial for SLAM. To this end, we compare the robot's performance when it is acting in active, passive, and fused modes and perform a sensitivity analysis over the range of parameters using Monte Carlo simulations. Showing that fused sensing can benefit SLAM may open a new paradigm for sonar implementation in canonical engineering problems. In the next section, we present a simplified model of the robot motion and different sensing modes.

## 3 | MODELLING

Here, we assume a simple model for the robot in which its motion can be determined by its translational and rotational velocities:

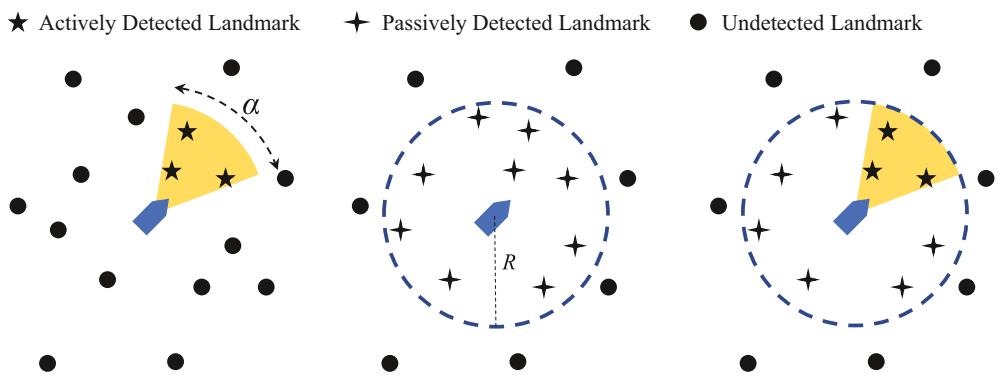


**FIGURE 1** A schematic figure of different sensing strategies. Active sonar (left) provides range and bearing information of the landmarks located within sensor opening $\alpha$. Passive sonar (middle) can only measure bearing angle omnidirectionally if the landmark is located within some distance $R$ of the sensor. Fused active and passive sonar (right) measures range and bearing to the landmarks within the sensor's opening $\alpha$ and the bearing to other landmarks within distance $R$

$$
\begin{aligned}
x^r_{k+1} &= x^r_k - \frac{v_k}{w_k}\sin(\phi_k) + \frac{v_k}{w_k}\sin(\phi_k + w_k dt) + \nu^x_k, \\
y^r_{k+1} &= y^r_k - \frac{v_k}{w_k}\cos(\phi_k) + \frac{v_k}{w_k}\cos(\phi_k + w_k dt) + \nu^y_k, \quad (1) \\
\phi_{k+1} &= \phi_k + w_k dt + \nu^\phi_k,
\end{aligned}
$$

where $x^r_k$, $y^r_k$, and $\phi_k$ are respectively the $x$, $y$ coordinates and orientation of the robot, $v_k$ and $w_k$ are respectively the translational and rotational velocities, $\nu^x_k$, $\nu^y_k$, $\nu^\phi_k$ are the corresponding components of the process noise vector sampled from a Gaussian distribution with covariance $\mathbf{Q}_k$, and $dt$ is the discretization time step.

The robot can only sense the sound if the sound source is located within a range $R$ of the robot and within a circular section with opening angle $\alpha$ modelling the main lobe of the sonar's emitter. We assume the receivers are omnidirectional and therefore that the bearing angle of the sound source can be measured omnidirectionally. Thus, the passive sonar is able to measure the bearing angle of the sound source or a reflector as long as it is located within the range $R$ from the robot. A schematic of different sensing mechanisms is illustrated in Figure 1.

## 4 | SIMULTANEOUS LOCALIZATION AND MAPPING USING EXTENDED KALMAN FILTER

As mentioned before, we tackle the landmark-based SLAM problem. Among all the methods developed to solve the SLAM problem, we use the approach based on an EKF, that is, EKF–SLAM, for several reasons. The EKF–SLAM is one of the most common algorithms to solve SLAM. In addition, this algorithm is relatively inexpensive computationally, especially for small maps where the covariance matrices are small. This makes it easier to perform Monte Carlo simulations to compare the performance of different measurement strategies. Finally, the performance of the EKF algorithm is affected by the availability of new measurements. Because this algorithm is based on linearization about the best estimates of the states, we expect this algorithm will be able to clarify the differences between different sensing strategies.

In two-dimensional landmark-based SLAM, the state vector contains the location and orientation of the robot as well as the locations of landmarks. Because we assume the landmarks are stationary, the only changing part of the dynamic equation corresponds to the robot and is stated in Equation (1). We assume that the data association is known for the sake of simplicity in comparing performance of using different sensing approaches. Assuming known association is common in bearing-only SLAM using cameras based on the colour or other features of the landmarks [45–47]. However, based on the current state of the art, it is more challenging to extract acoustic features of the reflector from the received echo, even though bats appear to be able to deal with the challenge. As another example, a recent study uses a feature extraction algorithm for object detection in a sonar image [48]. In addition, there are general techniques for data association such as the use of Mahalanobis distance [34] and joint probabilistic data association [49]. In the bearing-only SLAM, the data association is more challenging because the location of landmarks cannot be found by a single measurement. Several algorithms have been suggested to solve data association, such as data association based on clustering without using any feature information [50] or a combination of hypothesis testing and some feature information such as [51, 52].

In the following sections, we briefly summarize the EKF–SLAM algorithm using active sonar, passive sonar, and the fusion of these sensing approaches.

### 4.1 | EKF-SLAM with active sonar

As stated before, while using active sensing, the robot has access to range and bearing information of each landmark within the circular segment of sensing, and EKF–SLAM is one of the most common algorithms using range and bearing

measurement [34]. In this case, the measurement vector, $\mathbf{z}_k$, is the augmentation of the range and bearing measurement $\mathbf{z}_k^j$ from all landmarks $j$ in the sensing region:

$$\mathbf{z}_k^j = \begin{bmatrix} \sqrt{\delta x^2 + \delta y^2} \\ \arctan\left(\frac{\delta y}{\delta x}\right) - \phi_k \end{bmatrix} + \boldsymbol{\omega}_k, \tag{2}$$

where $\delta x$ and $\delta y$ are the horizontal and vertical distances between the robot and the $j^{\text{th}}$ landmark, respectively, and $\boldsymbol{\omega}_k$ denotes the measurement vector noise sampled from a Gaussian distribution with covariance $\mathbf{R}_k$. This equation is obtained by using the geometric relation between robot and landmark location and the range and bearing measurement and solving it for the range and bearing values. Because active sonar can provide both range and bearing, this equation can be solved even with only a single measurement sample. Therefore, only one measurement is sufficient to initialize the location of the landmark.

If $\widehat{\mathbf{x}}_k$ denotes the estimation of the state vector at time step $k$, and $\mathbf{P}_k$ is its covariance, the state estimation vector and its covariance at the next time step can be found by

$$\begin{aligned} \widehat{\mathbf{x}}_{k+1} &= \bar{\mathbf{x}}_{k+1} + \bar{\mathbf{P}}_{xz}\bar{\mathbf{P}}_{zz}^{-1}(\mathbf{z}_{k+1} - \bar{\mathbf{z}}_{k+1}), \\ \mathbf{P}_{k+1} &= \bar{\mathbf{P}}_{k+1} - \bar{\mathbf{P}}_{xz}\bar{\mathbf{P}}_{zz}^{-1}\bar{\mathbf{P}}_{xz}^T, \end{aligned} \tag{3}$$

where $\bar{\mathbf{x}}_{k+1}$ and $\bar{\mathbf{P}}_{k+1}$ are respectively the predicted state and its covariance, $\bar{\mathbf{z}}_{k+1}$ is the predicted measurement, which is an augmentation of the predicted measurement of each landmark as calculated in Equation (2), and $\bar{\mathbf{P}}_{zz}$ is the augmented measurement covariance containing the sensor noise covariances for each landmark measurement. Finally, $\bar{\mathbf{P}}_{xz}$ is the predicted covariance of measurement with state, and $\widehat{\mathbf{x}}_{k+1}$ and $\mathbf{P}_{k+1}$ are the estimated state and its covariance at time step $k+1$, respectively. More detail on calculation of the EKF can be found in [53].

## 4.2 | EKF-SLAM with passive sonar

In contrast to active sonar, passive sonar does not have access to range measurement, and therefore only the bearing angle measurement is accessible. In this case, the measurement equation is

$$\mathbf{z}_k^j = \arctan\left(\frac{\delta y}{\delta x}\right) - \phi_k + \omega_k, \tag{4}$$

where $\delta x$ and $\delta y$ are the horizontal and vertical distances between the robot and the $j^{\text{th}}$ landmark, respectively, and $\omega_k$ denotes the bearing angle measurement noise sampled from a Gaussian distribution with variance $\sigma_{\theta k}^2$.

Because passive sonar is a bearing-only sensor, the location of a landmark cannot be estimated using a single measurement, and therefore, Equation (4) cannot be used to find the predicted measurement $\bar{\mathbf{z}}_{k+1}$. Thus, it is necessary to initialize the landmark location before performing the EKF. This is a challenge in performing bearing-only SLAM, and several solutions have been presented in the literature. A good summary and comparison of these methods is presented in [54]. We use the method introduced in [50]. In this approach, the landmark location is represented by a Gaussian distribution in the plane. The centre of this distribution is defined as the intersection of bearing direction lines measured from two different robot positions. Knowing the centre point of the distribution from each robot location, the covariance of the location of the landmark can be estimated assuming a large range covariance and using the bearing angle measurement noise covariance and then applying the appropriate change in the coordinates and translating the covariance of the robot location based on the method derived in [55]. Finally, the covariance of the landmark location can be found by fusing the covariance matrices estimated from each of the different robot locations. Because initialization accuracy improves when the apex angle formed between two robot locations and the landmark is large, we only start initiating a landmark after detecting it passively in five consecutive measurements, using the first and last robot locations for initialization.

After each landmark is initialized, the landmark location and its covariance are augmented in the state vector and the covariance matrix to perform one step of Kalman filter estimation according to Equation (3) with associated measurement values. We should note here that in augmenting the covariance of the new landmark to the state covariance matrix, we follow the approach in [50], in which we simply add the landmark covariance as a diagonal term to the state covariance matrix to ensure that the state covariance remains positive definite. In other words, we assume that the uncertainty of the newly detected landmark is independent from the uncertainty of the other landmarks. We note that this assumption is not accurate because the landmark covariances are coupled through the robot location. However, this assumption is not detrimental to the entire estimation process because it is only applied in initialization steps, and the strength of this coupling emerges in the future iterations of the EKF algorithm.

## 4.3 | EKF-SLAM fused sonar

Active sonar has the advantage of range measurement, while passive sonar has the advantage of being omnidirectional. The motivation behind combining active and passive sonar measurement is to exploit the advantages of the two measurement approaches to improve the performance of the robot. This combination resembles the eavesdropping that may be used by bats during their group flights; however, to the best of our knowledge, it has not been implemented along with active sonar in robotic systems.

In this mode, the robot has access to the range and bearing measurement of the landmarks located within the active sonar beam pattern, which is modelled by a circular sector, as well as

the bearing measurement from landmarks within range distances through passive sonar. Therefore, the measurement equation is the augmentation of the measurement equations of active sonar and passive sonar presented in Equations (2) and (4), respectively. The landmarks detected using passive sonar are initialized through the same process explained in the previous section. When the state vector and its covariance become available, we can perform an EKF update as presented in Equation (3).

## 5 | SIMULATION RESULTS

### 5.1 | Simulation setup

To evaluate the performance of the different sensing strategies for different parameter values, we numerically simulate the EKF–SLAM algorithm in each sensing mode. The robot is placed in an environment with a regular rectangular array of landmarks with horizontal and vertical distances of 1 and 2 m, respectively. The array is large enough that the robot will never reach the boundary during simulation time. This way, under all simulation conditions, the robot explores an area with constant landmarks density by being away from the edges of the landmark array. Therefore, simulation results will not be affected by landmark density in the environment.

Because there are random parameters in the system, we perform a Monte Carlo simulation of 1000 repetitions. The initial location of the robot is selected randomly with uniform density within a box around the central landmark such that the closest landmark to each point in the box is the central landmark. Therefore, within a large grid of landmarks that contains the robot during the simulation time, this selection of initial conditions samples from all possible cases within the entire grid. In addition, the initial orientation of the robot is selected randomly from a uniform distribution between 0 and $2\pi$ radians. Figure 2 shows a sample snapshot of the simulation.

The parameters used in these simulations are related to either the robot or the sensor. The robot parameters are the translational speed $v_k$, rotational speed $w_k$, and the standard deviations of the robot's horizontal and vertical position noises and rotational noise. The sensor parameters are standard deviations of range and bearing measurement noises and the opening angle of the active sonar. All noise values are assumed to have a zero-mean Gaussian distribution.

In order to perform a fair comparison, in each Monte Carlo simulation, the robot parameters, initial condition, and process noise realizations are set to be identical between different sensing strategies. In addition, because the bearing measurement in all strategies uses the time difference of arrival, the bearing measurement noise realization is considered identical in all cases. In addition, the range measurement noise realization is set to be equal in the active and fused sensing strategies. To compare the effectiveness of different strategies, we perform simulations for different values of standard deviation of bearing measurement noise and active sonar opening angle while keeping the accuracy of range measurement constant.

Because the translational and rotational speed of the robot is assumed to be constant, the robot tries to move on a circle, but the actual path is not a perfect circle because of the process noise. The simulation stops if no new landmarks are detected within a termination window of 600 time steps, which is more than the time required for the robot to close the loop. Table 1 summarizes the numerical values of all parameters used in the numerical simulation.

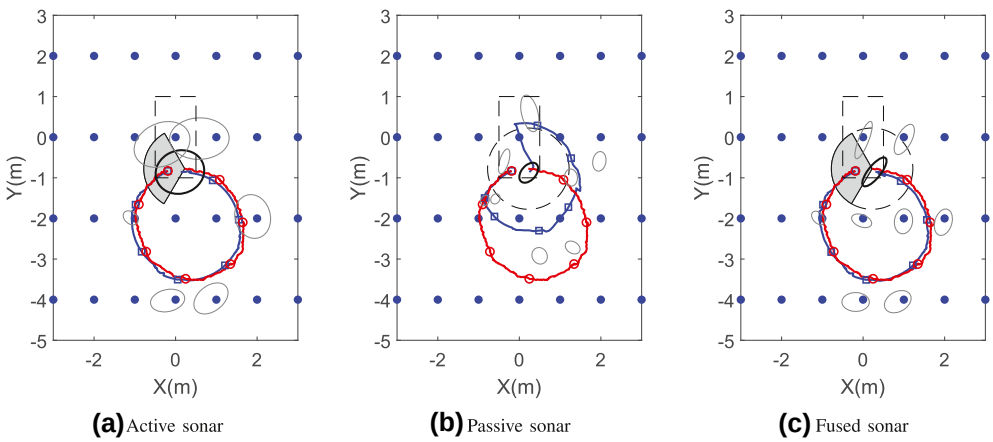


**FIGURE 2** A snapshot of the simulation. The paths in the left, middle, and right figures are associated with the EKF–SLAM solution when the robot is using active sonar, passive sonar, and fused sonar, respectively. The shaded circular sector centred at the robot location shows the opening angle of the active sensing, which only presented in active and fused sonar cases. The dashed circle centred around the robot shows the region where robot can sense using passive sonar. The dashed rectangle at the origin shows the region where the initial location of the robot is sampled uniformly from in each Monte Carlo simulation. The grid of blue circles shows the landmarks present in the environment. The red path with circular markers is the real path the robot is taking and is identical in all three cases. The blue paths with rectangular markers are the estimated path of the robot found through localization. The confidence region of the robot position is shown by the solid black ellipse around robot's estimated location. The confidence region of landmark estimation is shown with grey ellipses, where the estimated landmark locations are at the centres

**TABLE 1** Simulation parameters

| Variable | Symbol | Value |
|---|---|---|
| Time step | $dt$ | 1/10 s |
| Translational speed | $v_k$ | 0.2 m/s |
| Rotational speed | $w_k$ | 0.15 rad/s |
| Number of landmarks | - | 81 |
| Number of repetitions | $N$ | 1000 |
| Standard deviation of robot's x, y position noise | $\sigma_x$, $\sigma_y$ | 0.01 m |
| Standard deviation of robot's orientation noise | $\sigma_\phi$ | 0.0075 rad |
| Sensing range | $R$ | 1 m |
| Active sonar opening angle | $\alpha$ | $[\frac{\pi}{10}, 2\pi]$ rad |
| Standard deviation of range measurement noise | $\sigma_r$ | 0.01 m |
| Standard deviation of bearing angle measurement noise | $\sigma_\theta$ | $[\frac{\pi}{900}, \frac{\pi}{6}]$ rad |
| Total time steps in averaging window | $N_w$ | 600 |
| Total time steps in termination window | - | 600 |

## 5.2 | Metrics

In this section, we evaluate the performance of EKF–SLAM using different sensing strategies. To this end, we compare the simulation results to answer three general questions: Which strategy reports more information about the landmarks in the environment, which strategy estimates the robot location more accurately, and finally, which strategy does a more accurate estimation of its state vector during the final stage of the simulation? In the following, we define metrics to evaluate these performance criteria. Each metric is evaluated for all the Monte Carlo simulations, and their average is used for comparison.

As mentioned before, the robot terminates its operation when it does not detect a new landmark for 600 time steps. Therefore, the termination time, $K_{\max}$, can be different and can be used as a metric of how quickly the robot can scan the environment. In addition, the number of landmarks a robot can report at the end of the simulation, $N_{\max}$, is also an important metric of how effectively the robot can scan the environment. We use these two metrics to evaluate the effectiveness of different sensing strategies to explore the environment.

To evaluate the accuracy of different sensing strategies in localizing the robot, we use the truth model to calculate the least squared errors in the robot's location and its heading angle calculated over the window of the last 600 time steps. In other words, for robot location, we calculate

$$\Delta\rho = \sqrt{\frac{\sum_{k=K_{\max}-N_w+1}^{K_{\max}} \left[\left(\widehat{x}_k^r - x_k^r\right)^2 + \left(\widehat{y}_k^r - y_k^r\right)^2\right]}{N_w}}, \tag{5}$$

where $\Delta\rho$ is the root mean squared error (RMSE) in robot location, and $\widehat{x}_k^r$ and $\widehat{y}_k^r$ are the estimated two-dimensional coordinates of the robot location at time step $k$, respectively. The true location of the robot at time step $k$ is known through the truth model to equal $x_k^r$ and $y_k^r$. The simulation length is $K_{\max}$, and $N_w$ denotes the length of the averaging window, which is set to be 600 time steps. Similarly, for the robot's heading, we find

$$\Delta\phi = \sqrt{\frac{\sum_{k=K_{\max}-N_w+1}^{K_{\max}} \left(\widehat{\phi}_k - \phi_k\right)^2}{N_w}}, \tag{6}$$

where $\Delta\phi$ is the RMSE in the robot's heading, and $\widehat{\phi}_k$ and $\phi_k$ are the estimated and true values of the robot's heading at time step $k$, respectively.

We compare the performance of the EKF using different sensing strategies in estimating the associated state vector. Because the number of landmarks detected by different sensing strategies can be different, to make a fair comparison, we only include the landmarks that have been detected by all the sensing strategies into the state vector. We use the RMSE of state vector over the averaging window:

$$\Delta\mathbf{x} = \sqrt{\frac{\sum_{k=K_{\max}-N_w+1}^{K_{\max}} \|\widehat{\mathbf{x}}_k - \mathbf{x}_k\|^2}{N_w}}, \tag{7}$$

where $\widehat{\mathbf{x}}_k$ and $\mathbf{x}_k$ are the estimated state and the true state at time step $k$, respectively. In addition to the accuracy of estimation, we also evaluate the confidence of the estimation by calculating the maximum eigenvalue of the covariance matrices and the Frobenius norm of the covariance matrix calculated by the EKF in different sensing strategies.

Finally, we evaluate the consistency of the estimation using different sensing strategies by the chi-squared filter

performance metric [53]. First, we calculate the normalized estimation error squared (NEES) at each time step:

$$\chi_k = (\widehat{\mathbf{x}}_k - \mathbf{x}_k)^T \mathbf{P}_k^{-1} (\widehat{\mathbf{x}}_k - \mathbf{x}_k). \tag{8}$$

If the filter is consistent, then the estimation error becomes a sample from a zero-mean distribution with covariance $\mathbf{P}_k$. Therefore, the NEES calculated in Equation (8) should be a sample from a chi-squared distribution of degree equal to the degree of the state vector. Otherwise, the covariance $\mathbf{P}_k$ reported by the EKF is not a good representation of the actual covariance of the estimation. Therefore, it is possible to evaluate the consistency of the filter by counting the number of simulations for which the NEES calculated by Equation (8) deviates from the statistics of a chi-squared distribution, given an acceptable deviation region. If too many cases deviate from the chi-squared distribution, the estimation covariance is not a good representative of the true accuracy of the filter. It is a well-known disadvantage of the EKF that it tends to face consistency issues and be overconfident; in other words, the filter reports a wrong estimate of the state vector with small confidence regions [56]. This metric is designed to identify those errors if they occur.

## 5.3 | Results

The simulation results are presented in this section. We report the RMSE in robot localization, the maximum number of detected landmarks during the simulation time, the RMSE of the location of landmarks detected by all the sensing scenarios, the maximum eigenvalue of the state estimation error covariance, and the chi-squared consistency test of the state estimation.

### 5.3.1 | Robot localization accuracy

The RMSE in the robot's location is shown in Figure 3, when the robot only uses active sonar (Figure 3a), when it only uses passive sonar (Figure 3b), and when it fuses active and passive sonar (Figure 3c). We can see from this figure that when the robot only uses active sonar with a constant opening angle, the robot localization error increases as the covariance of bearing angle measurement increases. At constant covariance of the bearing angle measurement noise, the error decreases as the opening angle increases, and the rate of change in the error is higher in smaller opening angles.

As shown in Figure 3b, when the robot only uses passive sonar, the error in the robot's location is approximately constant for each opening angle, but the error is larger for very small bearing measurement noise covariance.

Finally, Figure 3c shows that when the robot fuses the information of active and passive sonar, the error in the robot's location is almost always smaller in magnitude than when it only relies on active sonar for all values of $\alpha$ and $\sigma_\theta$. In contrast, comparison of the fused sonar and passive sonar scenarios shows that the error in the robot's location is only smaller in fused sonar for very small values of $\sigma_\theta$.

The RMSE of the robot's heading angle for different sensing strategies shows a pattern similar that reported in Appendix 8.

### 5.3.2 | Landmark detection

As mentioned before, the robot terminates its search when it does not detect a new landmark for 600 time steps, and we denote the number of time steps it takes for the robot to finish its search by $K_{\max}$. The simulation results show that using different sensing strategies does not make a significant difference between them (not shown). However, as shown in Figure 4, the number of detected landmarks $N_{\max}$ is less by up to a factor of 3 when active sensing with small opening angles is used compared with passive or fused sensing. Otherwise, this number is insensitive to the opening angle.

### 5.3.3 | State estimation

The RMSE in localization of the landmarks detected by all the sensing mechanisms is shown in Figure 5. This plot shows the

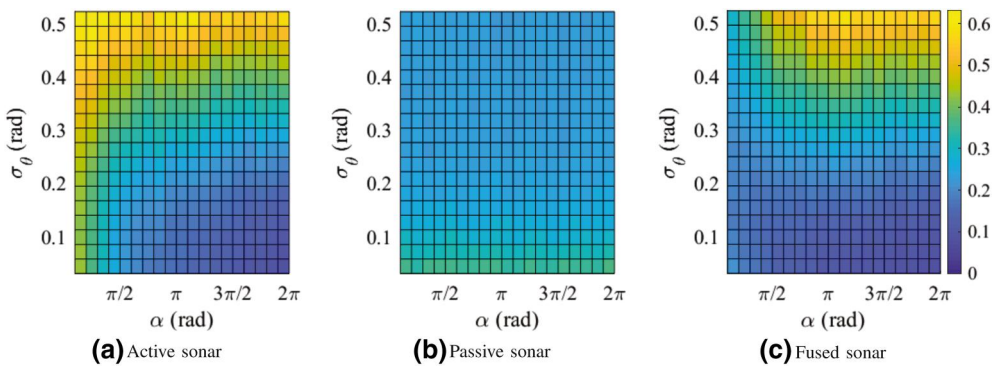


**FIGURE 3** Root mean squared error of the robot location for (a) active sonar, (b) passive sonar, and (c) fused sonar varying the opening angle $\alpha$ and bearing angle measurement covariance $\sigma_\theta$

same general pattern of the RMSE in robot localization as shown in Figure 3. In the active and fused sonar cases, the RMSE value increases as the opening angle increases at a constant $\sigma_\theta$. This error also increases as $\sigma_\theta$ increases at a constant opening angle. In passive sonar case, the RMSE is almost constant but it is relatively smaller for very small values of opening angle $\alpha$ and is relatively larger for very small values of $\sigma_\theta$.

Figure 6 shows the maximum eigenvalue of the estimation error covariance for different sensing strategies. For active sonar, the maximum eigenvalue of the estimation error covariance gets smaller as the opening angle increases, but it is approximately constant as the bearing angle measurement noise changes. This metric is significantly higher in passive sonar, especially for higher values of $\sigma_\theta$. Fused sonar is similar to active sonar except for small opening angle and significant $\sigma_\theta$, which shows higher values in comparison with active sonar, and for small $\sigma_\theta$ and opening angles less than $\pi$, which shows smaller values. Also for each parameter, the value of this metric in fused sonar is always less than or equal to its corresponding value in passive sonar.

The results of the chi-squared test are shown in Figure 7. This metric is more or less equivalent in active and fused sonar, except for very small values of $\alpha$ and $\sigma_\theta$, where active sonar shows smaller values. The chi-squared test value decreases monotonically for passive sonar as $\sigma_\theta$ increases.

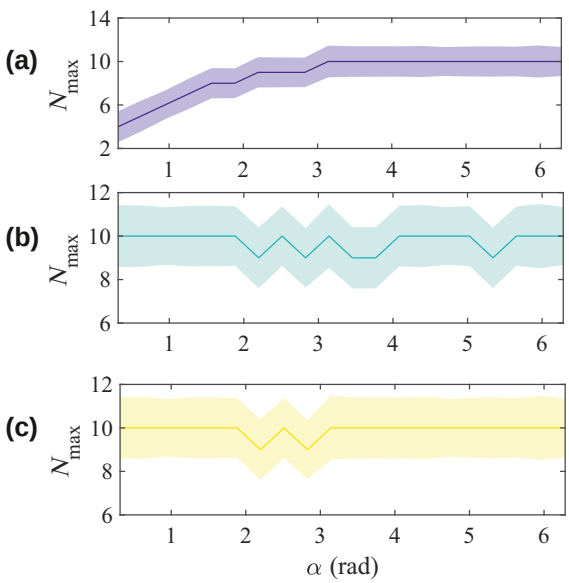


**FIGURE 4** Maximum number of landmarks detected by (a) active sonar, (b) passive sonar, and (c) fused sonar. The lines show the mean over the Monte Carlo simulations, and the shaded area shows ± one standard deviation

## 6 | DISCUSSION

In this section, we investigate which sensing mechanism performs better overall in solving the SLAM problem based on the calculated metrics reported in the results section. Based on the defined metrics, an estimation algorithm performs well if it has low robot localization RMSE, low landmark localization RMSE, a high number of detected landmarks, low maximum eigenvalue of the estimation covariance matrix, and low value in the chi-squared performance test. Here, we divide the simulation parameters into four different regions: high $\sigma_\theta$ and high $\alpha$, high $\sigma_\theta$ and low $\alpha$, low $\sigma_\theta$ and high $\alpha$, and low $\sigma_\theta$ and low $\alpha$. Then, we compare the performance of each sensing mechanism for each parameter region.

### 6.1 | High $\sigma_\theta$ and high $\alpha$

When $\sigma_\theta > 0.3$ radians (about 17°) and $\alpha > \pi$, Figures 3 and 5 show that the RMSE in robot and landmark localization increases in active and fused sensing, and therefore, one might consider passive sonar a better sensing strategy. However, according to Figure 6, the estimation algorithm based on passive sonar is not confident about its estimation. Recall that, because of the lack of range measurement in passive sonar, a landmark is localized after being detected in five different measurements by fusing the information of the first and fifth measurement. This will reduce the sensitivity of landmark initialization to bearing angle measurement noise in comparison with active sonar initialization that relies on only one bearing angle

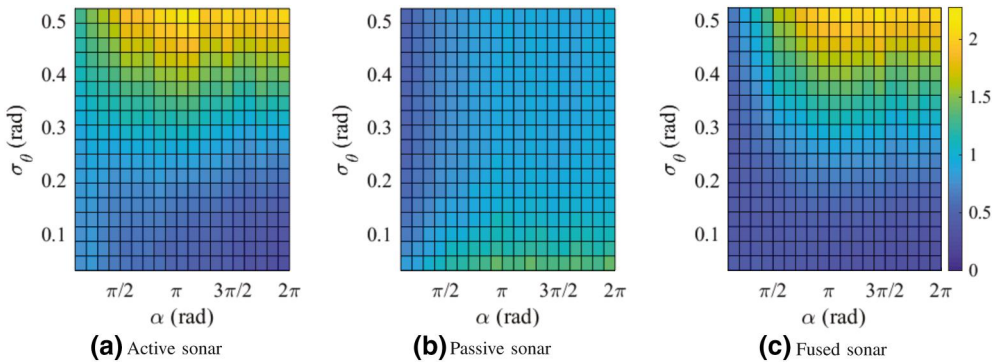


**FIGURE 5** Root mean squared error of the estimated location of the landmarks detected by all sensing mechanisms for (a) active sonar, (b) passive sonar, and (c) fused sonar varying opening angle $\alpha$ and bearing angle measurement covariance $\sigma_\theta$

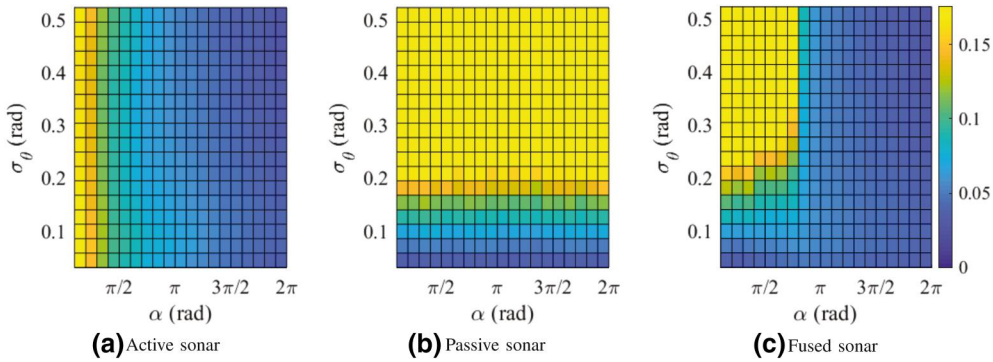


**FIGURE 6** Maximum eigenvalue of the state estimation covariance matrix for (a) active sonar, (b) passive sonar, and (c) fused sonar varying opening angle $\alpha$ and bearing angle measurement covariance $\sigma_\theta$

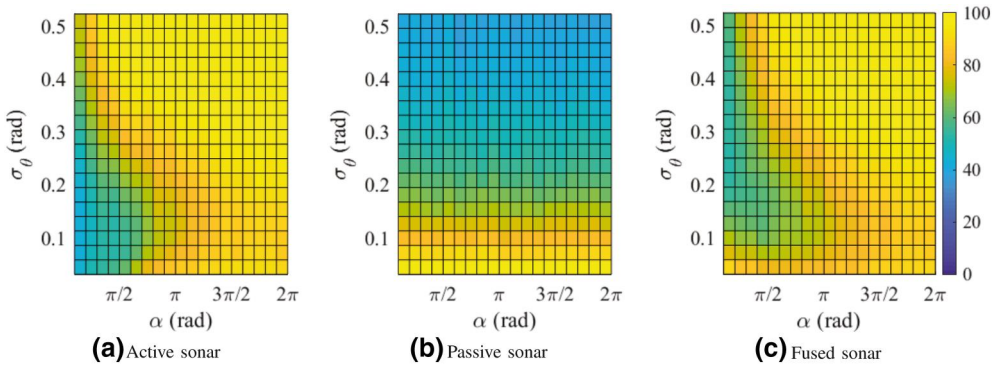


**FIGURE 7** Chi-squared filter performance test for (a) active sonar, (b) passive sonar, and (c) fused sonar varying opening angle $\alpha$ and bearing angle measurement covariance $\sigma_\theta$

measurement. Therefore, an offset in bearing angle measurement can create large errors in localizing a landmark (especially for those located farther from the robot), and the EKF may not be able to correct it because of a small Kalman gain caused by a lack of confidence in the measurement. This can explain the smaller localization and mapping errors observed in the case of passive sonar in comparison with those of active and fused sonar.

Figure 4 shows that all the sensing strategies perform similarly in detecting the landmarks around them. This result is expected because, at large sensing angles, active sonar acts similarly to an omnidirectional sensor while passive and fused sonar are omnidirectional. For this reason, one may expect all the sensing mechanisms detect the exact number of landmarks when the opening angle is large. However, Figure 4 shows that passive sonar performs slightly worst on average. This is the result of initialization approach used in passive sonar, which requires a landmark to be observed at least five times to be detected. On the other hand, a landmark only requires one measurement to be localized using active sonar. This is the reason that some landmarks will not be detected using only passive sonar, but they are detected by active or fused sonar.

Finally, according to Figure 7, both active and fused sonar perform poorly according to the chi-squared test, but passive sonar shows better response. However, the lower chi-squared test value in passive sonar is merely due to large covariances in state estimation that leads to a small value of NEES (Equation (8)). Therefore, a low chi-squared test by itself does not indicate a better performance of the EKF estimator using only passive sonar. In summary, for this region of parameters, none of the sensing mechanisms lead to an estimator with acceptable performance because of very high bearing angle measurement noise covariance that corrupts the sensor measurement.

## 6.2 | High $\sigma_\theta$ and low $\alpha$

When $\sigma_\theta > 0.3$ and $\alpha < \pi$, the passive sensing robot performance is similar to the previous case, that is RMSE in robot (Figure 3) and landmark localization (Figure 5) are small, yet the robot's state estimation is not confident as is evident by large maximum eigenvalue of the covariance of state estimation error (Figure 6). This is expected because the robot performance using omnidirectional passive sonar should not depend on the opening angle $\alpha$. Comparison of the RMSE in robot and landmarks localization for active and fused sonar simulations shows that fused sonar has smaller error yet shows less confidence in the state vector estimation that manifests in large maximum eigenvalue of estimation error covariance. It shows that for small opening angles, the fused sonar performance is influenced more by passive sonar. However, the high value of

$\sigma_\theta$ leads to poor performance that manifests as large confidence regions.

Figure 4 shows that fused sonar is better at detecting landmarks than active sensing is. This result is expected because fused sonar exploits the omnidirectionality of passive sonar that compensates for the limited view angle of the active sonar. The chi-squared test result also shows that the fused sonar performs slightly better than the active sonar; however, this is also due to its large estimation covariance. Thus, when the opening angle is small, the fused sensing inherits the properties of both active and passive sonar.

### 6.3 | Low $\sigma_\theta$ and high $\alpha$

When $\sigma_\theta < 0.3$ and $\alpha > \pi$, among different sensing strategies, passive sonar has the highest value of RMSE in robot and landmark locations while active sonar and fused sonar show the same performance according to Figures 3 and 5. Figure 5 shows that all sensing mechanisms perform the same in finding landmarks around them. This result in this region is expected because, when the robot uses active or fused sonar, it has access to range measurement in contrast to the passive sonar, which only measures bearing angle. In addition, the bearing angle noise measurement is small enough to allow acceptable localization of the landmark. According to Figure 6, all the sensing mechanisms show a good confidence in their estimation, yet the passive sonar loses confidence sooner as $\sigma_\theta$ increases. Finally, again due to implementation of EKF, none of the sensing approaches perform well according to the chi-squared consistency test. Therefore, as a summary, both active and fused sensing strategies perform similarly as expected, because with large opening angle, fused sonar mostly relies on active sonar information. Therefore, in this region, the information provided by the passive sonar is more or less redundant.

### 6.4 | Low $\sigma_\theta$ and low $\alpha$

This is the region of parameter space where implementing fused sensing is beneficial. Comparing Figures 3 and 5 shows that fused sonar has the smallest RMSE in robot and landmark localization compared with that of active and passive sonar. In addition, Figure 6 shows that the estimation algorithm using fused sonar has more confidence in its estimation. The chi-squared consistency test shown in Figure 7 suggests similarity between active and fused sonar. Again, we should notice here that although active sonar seems to have better consistency than fused and passive sonar, we believe that fused sonar outperforms the other strategies in this region. This is due to the higher confidence of the estimation when fused sonar is used compared with active and passive sonar, especially when $\sigma_\theta$ is between 0.1 and 0.2 rad. Finally, Figure 4 shows that fused sonar can detect more landmarks than active sonar. Therefore, in this parameter region, the fused sonar can detect more landmarks than active sonar, it can localize the landmarks that both algorithms detect more accurately, and it can localize the robot with more accuracy as well. In addition to lower error, the fused sonar case shows more confidence in its estimation and a slightly better consistency.

## 7 | CONCLUSION

To summarize, the simulation results show that the EKF algorithm can perform better in solving the SLAM problem using a fused sonar sensing strategy when the opening angle is less than $\pi$ and the standard deviation of the bearing angle measurement noise, $\sigma_\theta$, is less than 0.3 rad (about 17°). This relatively small opening angle is consistent with beam widths for currently used commercial sonar sensors (see [57]). We intentionally used a wide range for $\sigma_\theta$ to ensure that we see a response dominated by noise as our upper limit for $\sigma_\theta$. Therefore, the result of this study is promising in practical implications. Nevertheless, the implementation of this work in practice comes with challenges such as data association or signal jamming in the case of extension to a multiagent robotic system as mentioned in the introduction to this paper. We believe that this work addresses solutions for interesting challenges for engineers and scientists in different disciplines, and it may initiate a research path that will potentially alter the way we currently use sonar sensors for navigation.

**ACKNOWLEDGEMENT**

This work was supported by the National Science Foundation under grant CMMI-1751498.

**ORCID**

*Nicole Abaid* https://orcid.org/0000-0002-0053-4710

**REFERENCES**

1. Christensen, H.I., Hager, G.D.: Sensing and Estimation, pp. 91–112. Springer, New York (2016)
2. García, E., et al.: Spreading sequences in active sensing: a review. Signal Process. 106, 88–105 (2015)
3. Leonard, J.J., Durrant-Whyte, H.F.: Directed Sonar Sensing for Mobile Robot Navigation, vol. 175. Springer Science, Oxford (2012)
4. Kim, S., et al.: Performance comparison of target localization for active sonar systems. IEEE Trans. Aero. Electron. Syst. 44(4), 1371–1380 (2008)
5. Burguera, A., González, Y., Oliver, G.: Sonar sensor models and their application to mobile robot localization. Sensors. 9(12), 10 217–10 243 (2009)
6. Brown, M.: Feature extraction techniques for recognising solid objects with an ultrasonic range sensor. IEEE J. Robot. Autom. 1(4), 191–205 (1985)
7. Nagla, K.S., Uddin, M., Singh, D.: Improved occupancy grid mapping in specular environment. Robot. Autonom. Syst. 60(10), 1245–1252 (2012)
8. Kleeman, L., Kuc, R.: Sonar Sensing, pp. 753–782. Springer International Publishing, Cham (2016)
9. Barshan, B., Kuc, R.: Differentiating sonar reflections from corners and planes by employing an intelligent sensor. IEEE Trans. Pattern Anal. Mach. Intell. 12(6), 560–569 (1990)
10. Krammer, P., Schweinzer, H.: Localization of object edges in arbitrary spatial positions based on ultrasonic data. IEEE Sensor. J. 6(1), 203–210 (2006)

11. Walter, S.: The sonar ring: obstacle detection for a mobile robot. In: Proceedings of the 1987 IEEE International Conference on Robotics and Automation, vol. 4, pp. 1574–1579. IEEE, Raleigh (1987)
12. Fazli, S., Kleeman, L.: A real time advanced sonar ring with simultaneous firing. In: Proceedings of the 2004 IEEE/RSJ International Conference on Intelligent Robots and Systems (IROS) (IEEE Cat. No. 04CH37566), vol. 2, pp. 1872–1877. IEEE, Sendai (2004)
13. Tardós, J.D., et al.: Robust mapping and localization in indoor environments using sonar data. Int. J. Robot. Res. 21(4), 311–330 (2002)
14. Ribas, D., Ridao, P., Neira, J.: Underwater SLAM for Structured Environments Using an Imaging Sonar, vol. 65. Springer, Berlin (2010)
15. Chong, T.J., et al.: Sensor technologies and simultaneous localization and mapping (SLAM). Procedia Comput. Sci. 76, 174–179 (2015)
16. Kaushal, H., Kaddoum, G.: Underwater optical wireless communication. IEEE Access. 4, 1518–1547 (2016)
17. Surlykke, A., et al. (eds.): Biosonar. Springer, New York (2014)
18. Thomas, J.A., Moss, C.F., Vater, M.: Echolocation in Bats and Dolphins. University of Chicago Press, Chicago (2004)
19. Bates, M.E., Stamper, S.A., Simmons, J.A.: Jamming avoidance response of big brown bats in target detection. J. Exp. Biol. 211(1), 106–113 (2008)
20. Obrist, M.K.: Flexible bat echolocation: the influence of individual, habitat and conspecifics on sonar signal design. Behav. Ecol. Sociobiol. 36(3), 207–219 (1995)
21. Chiu, C., et al.: Effects of competitive prey capture on flight behaviour and sonar beam pattern in paired big brown bats, *Eptesicus fuscus*. J Exp Biol. 213(19), 3348–3356 (2010)
22. Fu, Y., Caspers, P., Müller, R.: A dynamic ultrasonic emitter inspired by horseshoe bat noseleaves. Bioinspiration Biomimetics. 11(3), 036007 (2016)
23. Yin, X., Müller, R.: Fast-moving bat ears create informative Doppler shifts. Proc. Natl. Acad. Sci. Unit. States Am. 116(25), 12 270–12 274 (2019)
24. Yang, L., Yu, A., Müller, R.: Design of a dynamic sonar emitter inspired by hipposiderid bats. J. Acoust. Soc. Am. 141(5), 3485 (2017)
25. Chan, Y.T., Ho, K.C.: A simple and efficient estimator for hyperbolic location. IEEE Trans. Signal Process. 42(8), 1905–1915 (1994)
26. Yang, K., Wang, G., Luo, Z.-Q.: Efficient convex relaxation methods for robust target localization by a sensor network using time differences of arrivals. IEEE Trans. Signal Process. 57(7), 2775–2784 (2009)
27. Kay, S., Vankayalapati, N.: Improvement of TDOA position fixing using the likelihood curvature. IEEE Trans. Signal Process. 61(8), 1910–1914 (2013)
28. Rascon, C., Meza, I.: Localization of sound sources in robotics: a review. Robot. Autonom. Syst. 96, 184–210 (2017)
29. Kuc, R.: Generating cognitive maps using echo features from a biomimetic audible sonar. J. Acoust. Soc. Am. 145(4), 2084–2093 (2019)
30. Rajai, P., et al.: Binaural sonar system for simultaneous sensing of distance and direction of extended barriers. IEEE Sensor. J. 19(24), 12 040–12 049 (2019)
31. Eliakim, I., et al.: A fully autonomous terrestrial bat-like acoustic robot. PLoS Comput. Biol. 14(9), e1006406 (2018)
32. Chiu, C., Xian, W., Moss, C.F.: Flying in silence: echolocating bats cease vocalising to avoid sonar jamming. Proc. Natl. Acad. Sci. Unit. States Am. 105(35), 13116–13121 (2008)
33. Corcoran, A.J., Conner, W.E.: Bats jamming bats: food competition through sonar interference. Science. 346(6210), 745–747 (2014)
34. Thrun, S., Burgard, W., Fox, D.: Probabilistic Robotics. MIT press, Cambridge (2005)
35. Du, T., et al.: Multi-sensor fusion SLAM approach for the mobile robot with a bio-inspired polarised skylight sensor. IET Radar, Sonar Navig. 14(12), 1950–1957 (2020)
36. Xu, Y., et al.: Robust and accurate UWB-based indoor robot localisation using integrated EKF/EFIR filtering. IET Radar, Sonar Navig. 12(7), 750–756 (2018)
37. Shinn-Cunningham, B.G., Santarelli, S., Kopco, N.: Tori of confusion: binaural localization cues for sources within reach of a listener. J. Acoust. Soc. Am. 107(3), 1627–1636 (2000)
38. Nguyen, Q.V., et al.: Localising an intermittent and moving sound source using a mobile robot. In: Proceedings of the 2016 IEEE/RSJ International Conference on Intelligent Robots and Systems (IROS), pp. 1986–1991. IEEE, Daejeon (2016)
39. Shirazi, M.J., Abaid, N.: Tracking a sound source with unknown dynamics using bearing-only measurements based on a priori information. In: Proceedings of the 2019 American Control Conference (ACC), pp. 4491–4496. IEEE, Philadelphia (2019)
40. Kneip, L., Baumann, C.: Binaural model for artificial spatial sound localization based on interaural time delays and movements of the interaural axis. J. Acoust. Soc. Am. 124(5), 3108–3119 (2008)
41. Cho, S.J., Ovcharenko, A., Chong, U.-P.: Front-back confusion resolution in 3d sound localization with HRTF databases. In: Proceedings of the 2006 International Forum on Strategic Technology, pp. 239–243. IEEE, Ulsan (2006)
42. Aytekin, M., et al.: The bat head-related transfer function reveals binaural cues for sound localization in azimuth and elevation. J. Acoust. Soc. Am. 116(6), 3594–3605 (2004)
43. Shim, Y., Park, J., Kim, J.: Relative navigation with passive underwater acoustic sensing. In: Proceedings of the 2015 12th International Conference on Ubiquitous Robots and Ambient Intelligence (URAI), pp. 214–217. IEEE, Goyang (2015)
44. Kwok, N.M., Dissanayake, G., Ha, Q.P.: Bearing-only SLAM using a SPRT based Gaussian sum filter. In: Proceedings of the 2005 IEEE International Conference on Robotics and Automation, pp. 1109–1114. IEEE, Barcelona (2005)
45. Lemaire, T., Lacroix, S., Sola, J.: A practical 3d bearing-only SLAM algorithm. In: Proceedings of the 2005 IEEE/RSJ International Conference on Intelligent Robots and Systems, pp. 2449–2454. IEEE, Edmonton (2005)
46. Ahmad, A., Huang, S., Dissanayake, G.: Accurate large-scale bearing-only SLAM by map joining. In: Proceedings of the 2010 Australasian Conference on Robotics and Automation. Brisbane (2010)
47. Deans, M.C., Hebert, M.: Bearings-only Localization and Mapping. Ph.D. dissertation, Citeseer (2005)
48. Tueller, P., Kastner, R., Diamant, R.: Target detection using features for sonar images. IET Radar, Sonar Navig. 14(12), 1940–1949 (2020)
49. Fortmann, T.E., Bar-Shalom, Y., Scheffe, M.: Multi-target tracking using joint probabilistic data association. In: Proceedings of the 1980 19th IEEE Conference on Decision and Control including the Symposium on Adaptive Processes, pp. 807–812. IEEE, Albuquerque (1980)
50. Costa, A., Kantor, G., Choset, H.: Bearing-only landmark initialisation with unknown data association. In: Proceedings of the 2004 IEEE International Conference on Robotics and Automation (ICRA'04), vol. 2, pp. 1764–1770. IEEE, New Orleans (2004)
51. Wang, C.-L., et al.: Bearing-only visual SLAM for small unmanned aerial vehicles in GPS-denied environments. Int. J. Autom. Comput. 10(5), 387–396 (2013)
52. Bryson, M., Sukkarieh, S.: Building a robust implementation of bearing-only inertial SLAM for a UAV. J. Field Robot. 24(1–2), 113–143 (2007)
53. Bar-Shalom, Y., Li, X.R., Kirubarajan, T.: Estimation with Applications to Tracking and Navigation: Theory Algorithms and Software. John Wiley & Sons, New York (2004)
54. Munguía, R., Grau, A.: Concurrent initialisation for bearing-only SLAM. Sensors. 10(3), 1511–1534 (2010)
55. Smith, R.C., Cheeseman, P.: On the representation and estimation of spatial uncertainty. Int. J. Robot. Res. 5(4), 56–68 (1986)
56. Psiaki, M.L.: The blind tricyclist problem and a comparative study of nonlinear filters: a challenging benchmark for evaluating nonlinear estimation methods. IEEE Contr. Syst. Mag. 33(3), 40–54 (2013)
57. Marine, T.: Acoustic Transducers. http://www.teledynemarine.com/acoustic-transducers (2013). Accessed November 2020


**How to cite this article:** Jahromi Shirazi M, Abaid N. Eavesdropping like a bat: Towards fusing active and passive sonar for a case study in simultaneous localization and mapping. *IET Radar Sonar Navig.* 2021;1–13. https://doi.org/10.1049/rsn2.12093

## APPENDIX A

The RMSE error of robot's heading using active, passive, and fused sonar is shown in Figure 8.

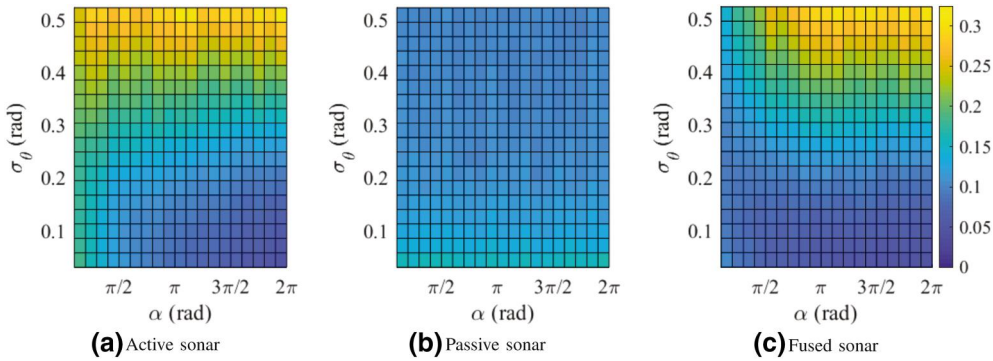


**FIGURE 8** Root mean squared error of the robot heading for (a) active sonar, (b) passive sonar, and (c) fused sonar varying opening angle $\alpha$ and bearing angle measurement covariance $\sigma_\theta$